AQUA
Water Infrastructure, Ecosystems and Society

IWA PUBLISHING

 AQUA — Water Infrastructure, Ecosystems and Society Vol 72 No 5, 633 doi: 10.2166/aqua.2023.120

Design of hydrodynamic cavitation-based advanced oxidation process for degradation of recalcitrant micropollutants originating from tertiary effluent streams: a case study with norfloxacin

Birupakshya Mishra[a], Abhishek Thaker[b], Anupam Mukherjee[a], Aditi Mullick[a], Subhankar Roy[b,*] and Siddhartha Moulik[a]

[a] Department of Process Engineering & Technology Transfer, CSIR-Indian Institute of Chemical Technology, Hyderabad 500007, India
[b] Department of Chemical Engineering, School of Energy Technology, Pandit Deendayal Energy University, Gandhinagar, Gujarat 382426, India
*Corresponding author. E-mail: subhankar.roy@sot.pdpu.ac.in

SR, 0000-0001-7132-4246

ABSTRACT

Treatment of micropollutants even after tertiary treatment and developing cost-effective, sustainable and energy-efficient technology for the same still remains an active area of research. The present study reports the feasibility and efficacy of hydrodynamic cavitation (HC)-based advanced oxidation process (AOP) for the degradation of norfloxacin. Experiments using HC were carried out in a sequential manner starting with the optimization of the cavitating device (orifice plate) using computational fluid dynamics (CFD) followed by optimizing the operational parameters such as pH, inlet pressure and initial concentration. An experimental study revealed that under optimized conditions of pH – 2, inlet pressure – 6 bar and initial conc – 250 μg/L, NRF degradation of 22.26% was obtained using HC in an experimental run of 60 min. For further improvement of the HC process, experiments were carried out by integrating with H_2O_2, O_3 and Fenton's reagent. Under the optimized conditions, integrating with H_2O_2, O_3 and Fenton's reagent enhanced the extent of NRF degradation. The energetics of the process was further evaluated to understand the techno-economic viability. The study revealed that HC + H_2O_2 consumed less energy of 8.01 kWh/m^3 at the economics of Rs. 82.53/m^3. Thus, HC combined with oxidizing agents can be a novel technique in the genre of AOP for the degradation of micropollutants.

Key words: advanced oxidation process, hydrodynamic cavitation, norfloxacin, synergistic effect, water treatment

HIGHLIGHTS

- CFD optimization study of orifice-based cavitating device.
- Micropollutant degradation using hydrodynamic cavitation coupled with other conventional means.
- The study of the synergistic effect of HC with H_2O_2.

1. INTRODUCTION

The industrial revolution has posed a significant risk to the aquatic environment by creating an imbalance between water demand and availability (Mukherjee *et al.* 2022a). In order to address the problem, environmental regulations such as the European Water Framework Directive (2000/60/EC), the North American Clean Water Act or the Water Law of the People's Republic of China have encouraged and invested in the implementation of wastewater treatment plants (WWTPs) as a mean to achieve 'Goal 6: Clean water and sanitation' and 'Goal 11: Sustainable cities and communities' of Sustainable Development Goals by United Nations (Department of Economic & Social Affairs n.d.). However, the increasing occurrence of recalcitrant micropollutants (MPs) in the aquatic environment after conventional wastewater treatment is still a major challenge and a top priority concern worldwide (Mukherjee *et al.* 2021a). WWTP is proposed to be a point source of MP, which enters the aquatic environment through industrial wastewater, domestic wastewater and storm water ranging in concentration levels from a few ng/L to several μg/L (Simha & Ganesapillai 2017). Extensive literature review carried out on the benefits and drawbacks of WWTPs indicates that MP's generated from the tertiary treatment point of pharmaceutical effluent

streams brings potential risk to aquatic and terrestrial organisms (Petrie *et al.* 2015; Ricky & Shanthakumar 2022). Intensive efforts for treatment of such recalcitrant MPs have been attempted by researchers worldwide using various physical (membrane filtration, flocculation, adsorption) (Das *et al.* 2020; Lanjewar *et al.* 2021), chemical (coagulation, electro-chemical oxidation) (Roy *et al.* 2020; Lanjewar *et al.* 2022) and biological methods (bacterial treatment, anaerobic digestion) (Maddela *et al.* 2020). However, these methods are designed to remove conventional pollutants (for instance, Chemical oxygen demand (COD) and nutrients) and are relatively less effective for MP removal. In addition, they possess several drawbacks such as (i) solid waste and side stream generation, (ii) slow reaction kinetics and high retention time and (iii) chemical consumption and high economics.

Thus, the current work is an effort towards introducing hydrodynamic cavitation (HC) as a tertiary treatment step to WWTP for MP degradation due to the huge potential inherent in the cavitation phenomenon. Moreover, compared with the existing advanced oxidation process (AOP), HC is more feasible in terms of sustainability, environment friendliness, less chance for harmful by-product formation and easy implementation at a pilot scale with huge effluent volume (Mukherjee *et al.* 2021b). A detailed literature review on the application of HC and other AOPs for the treatment of wastewater and degradation of MPs using various HC-based set-up is already presented in our previous works (Mukherjee *et al.* 2021c; Mishra *et al.* 2022a). In the present work, norfloxacin (NRF) originating mostly from the tertiary treatment point of pharmaceutical effluent streams is considered as a case study. NRF belongs to the family of fluoroquinolones and is used as an antibiotic in both human and veterinary medicine. 40–69% of the ingested NRF released from the body is in active form and is considered recalcitrant. Moreover, the extensive literature review on the deleterious effects of NRF is well reported (Gogate 2002; Chen *et al.* 2013). In this context, the multifold objectives of the present study are:

(i) Incorporation of HC for degradation of persistent organic MPs such as NRF.
(ii) Understanding and optimizing the geometric and operational parameters for better performance efficiency.
(iii) Understanding the degradation performance and kinetic studies by varying operating conditions.
(iv) Understanding integrated performance efficiency of HC along with other oxidizing agents such as ozone, hydrogen peroxide and Fenton's reagent.
(v) Understanding the process scalability by using techno-economic analysis and further paving the commercialization with maximum operational efficiency.

2. EXPERIMENTAL

2.1. Materials and equipment

2.1.1. Sample preparation

HPLC grade norfloxacin ($C_{16}H_{18}FN_3O_3$) of ≥98% purity with a molecular weight of 319.33 g/mol was obtained from M/S Sigma Aldrich Ltd, India. Demineralized water was prepared in the laboratory using a double-stage RO membrane which was used for the preparation of NRF solutions in varying ratios (w/v). Hydrochloric acid (37% w/v) was obtained from Avra Synthesis Pvt. Ltd, Hyderabad and was added dropwise until the desired pH was attained. Pelletized sodium hydroxide was obtained from Finar Chemicals, which was used to make the solution alkaline.

2.1.2. Oxidizing agents

Oxidizing agents like H_2O_2 were procured from Rankem Chemicals Haryana, India. Anhydrous ferrous sulphate to be used as Fenton's reagent was obtained from Sigma Industries, India. Ozone was generated using a commercial ozonator from Green Sun (Model Number: 3G118X) with an airflow rate of 1 LPM, ozone concentration of 50 g/m^3 and ozone flow rate of 3 g/h fitted with a sparger.

2.1.3. Elemental analysis

For Total organic carbon (TOC) analysis, ortho-phosphoric acid (H_3PO_4) and potassium hydrogen phthalate were procured from SD fine chemicals, Mumbai, India. Liquid chromatography–mass spectrometry (LCMS) was performed for quantification using 0.1% formic acid and acetonitrile nitrogen (N_2) was generated using a nitrogen generator (Peak N_2 generator) flow rate of 600 μl min^{-1}.

2.1.4. Experimental set-up

The schematic of the experimental set-up is discussed in our previous work (Mukherjee *et al.* 2020a). A feed tank of 50 L capacity was connected to a metering pump through a 50 mm internal diameter pipe. The solution from the pump is passed through the main line consisting of the cavitation device, across which pressure difference is produced. Two oil-filled pressure gauges (Baumer; max pressure 14 bar) were used for regulating pressure. Recycle line is provided in parallel to the main line and is used for regulating the flow rate by using a valve. A cooling jacket was provided to the reactor for maintaining the temperature at 25 ± 5 °C. The drain line is provided at the bottom of the tank for cleaning or sample collection. At the heart of the cavitating device, an orifice of 1.6 mm diameter of SS316 having 2 mm thickness. Oxidising agents such as H_2O_2 and Fenton's reagent are introduced in the tank in a single dose to avoid oxidation in atmosphere. Ozone was generated in the laboratory using a commercial ozonator system and was diffused inside the tank using a sparger. The process flow schematic has been depicted in Figure 1.

2.2. Numerical model

The Navier–Stokes equation is used as the first step in analyzing an axisymmetric, incompressible, viscous and homogeneous fluid. Since the inverse of the speed of sound squared is so small, the incompressible flow assumption looks quite reasonable. The governing equations of fluid flow are the continuity and the momentum equations. A two-phase fluid flow through the orifice is examined, which includes bulk liquid and vapour inside the cavities (Nasiruddin & Singh 2021). As a result, the simulation is done using the multiphase mixture approach. For each phase, a different set of governing equations is used. The mixture's governing equation and momentum equation can be written as follows:

$$\frac{\partial \rho_{\text{mix}}}{\partial t} + \vec{\nabla} \cdot (\rho_{\text{mix}} \cdot \vec{v}_{\text{mix}}) = 0 \tag{1}$$

where $\vec{v}_{\text{mix}}$ is the mean averaged velocity and is given by:

$$\vec{v}_{\text{mix}} = \sum_{i=1}^{n} \frac{\alpha_i \rho_i \cdot \vec{v}_i}{\rho_{\text{mix}}} \tag{2}$$

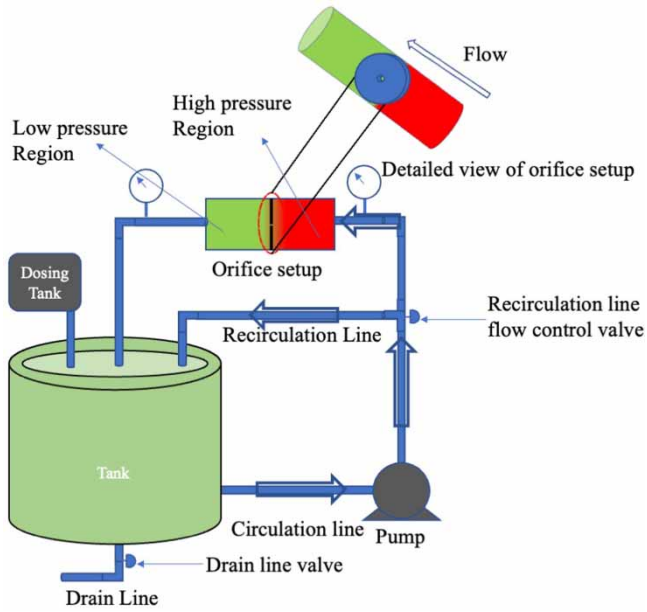

Figure 1 | Process flow schematic and experimental set-up.

where α_i is the volume fraction of phase i, n is the number of phases and ρ_{mix} is the density of mixture given by

$$\rho_{\text{mix}} = \sum_{i=1}^{n} \alpha_i \rho_i \tag{3}$$

The corresponding momentum equation is given by:

$$\frac{\partial}{\partial t}(\rho_{\text{mix}}\vec{v}_{\text{mix}}) + \nabla \cdot (\rho_{\text{mix}}\vec{v}_{\text{mix}}\vec{v}_{\text{mix}}) = -\nabla\rho + \nabla \cdot [(\mu_{\text{mix}} + \mu_{\text{t}})(\nabla\vec{v}_{\text{mix}} + \overrightarrow{\nabla v} T_{\text{mix}})] \tag{4}$$

where μ_{mix} is the viscosity of the mixture given by

$$\mu_{\text{mix}} = \sum_{i=1}^{n} \alpha_i \mu_i \tag{5}$$

Mass transfer between the liquid and vapour phases in the cavitation is given by:

$$\frac{\partial}{\partial t}(\rho_{\text{mix}} f) + \nabla \cdot (\rho_{\text{mix}}\vec{v}_v f) = \nabla \cdot (\gamma \nabla f) + R_a - R_c \tag{6}$$

where f is the vapour phase mass fraction, $\vec{v}_v$ is the vapour phase velocity, γ is the efficiency exchange coefficient, R_a is the vapourization rate and R_c is the condensation rate.

The rate of phase changes, vapourization and condensation are calculated from Rayleigh–Plesset equation (Singhal *et al.* 2002) and are given as:

$$\text{When,} \quad P < P_{\text{sat}}\,, \; R_a = C_a \frac{V_{\text{c}}}{\sigma} \rho_{\text{l}} \rho_v \sqrt{\frac{2(P_v - P)}{3\rho_{\text{l}}}}(1 - f) \tag{7}$$

$$\text{When,} \quad P > P_{\text{sat}}\,, \; R_c = C_c \frac{V_{\text{c}}}{\sigma} \rho_l \rho_l \sqrt{\frac{2(P - P_v)}{3\rho_{\text{l}}}}(f) \tag{8}$$

where V_{c} is the characteristic velocity representative of the effect of local relative velocity between liquid and vapour, σ is the surface tension coefficient, P_v is the vapour pressure, C_a and C_c are empirical constant (0.02 and 0.01).

The effect of turbulence on cavitation is given by

$$P_v = \left(P_{\text{sat}} + \frac{P'_t}{2}\right) \tag{9}$$

P_{turb} is the turbulent pressure fluctuation given by, $P'_t = 0.39\rho k$, where k is the turbulent kinetic energy.

The analysis took into account steady-state cavitation with no slip velocity near the wall. A mixture model is used to apply and simulate the Schnerr–Sauer model for multiphase flow (Kim *et al.* 1997). The vapour and liquid phases are treated as interpenetrating continuums in this paradigm. For the turbulence model standard, the k–ε scheme was explored. The SIMPLEC algorithm was used for pressure–velocity coupling, with 2nd order discretization applied to the density, momentum, vapour and turbulent kinetic energy as well as the turbulent dissipation rate in each instance and the residual for the continuity equation was set at 10^{-5} to ensure convergence. For vapour transport, a first-order scheme was used. The simulations were run at a constant outlet pressure of 1 atm.

Grid independency was ensured by calculating the pressure at the centre of the orifice as a function of the number of nodes (and elements) (Zhang & Li 2014). Refinement of grid did not have an impact on the pressure computed at the centre beyond 40,000 nodes as shown in Figure 2, where the pressure at the centre of the orificemeter is plotted for the different number of nodes. Therefore, further simulations were carried out using this particular number of nodes.

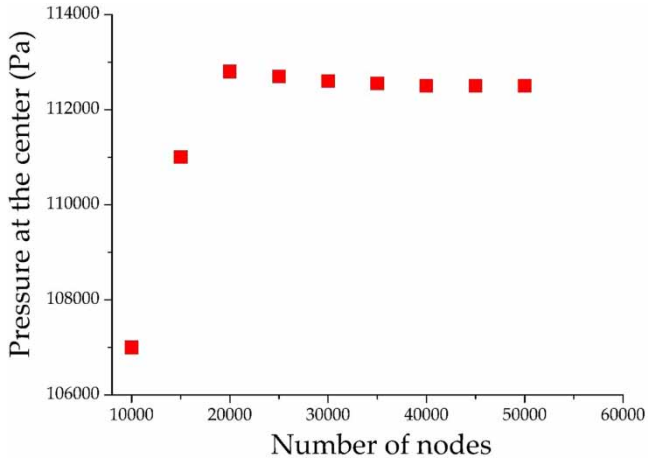

Figure 2 | Pressure at the centre of node vs. the number of nodes.

3. RESULTS AND DISCUSSION

3.1. Numerical optimization study

The dimensions of the orifice-based cavitating device as shown in the figure were investigated numerically and studies were carried out to calculate the ideal inlet-to-outlet pressure ratio, the ideal length of the orifice to the diameter of the orifice ratio (L/d) and the diameter of the inlet to the diameter of the orifice ratio (D/d). The effects of these parameters are studied by calculating the cavitation number to find out the extent of cavitation. Velocity and pressure profiles have been plotted for each corresponding pressure and L/d ratios (both as L constant and then as d constant) which are included in the Supplementary material.

3.1.1. Effect of the L/d ratio

The length of the orifice is an important parameter in determining pressure recovery at the outlet while the orifice diameter increases the velocity of the fluid. The ratio of the length of the orifice and the diameter of the orifice was varied to determine the effect of the said ratio on cavitation number. Initially, in the first phase of the numerical computations, L was fixed at 2 mm and d was varied, while in the next phase, the d was fixed at 1.6 mm and L was varied. The velocity profiles for changing L/d ratios are plotted in Supplementary Figure S1. It is observed that while initially there is an increase in velocity at the orifice as the diameter of the orifice decreases, the trend reverses at $L/d = 1.25$, beyond which the Ca number starts increasing. This is corroborated by Figure 3(a) which shows the variation of cavitation number with the L/d ratio. As the diameter of the orifice plate was decreased, starting from 4 mm, Ca first decreased to Ca = 0.29 at $L/d = 1.25$ before starting to rise again. It may be hypothesized that as the fluid flows through the constriction, an increase in flow velocity at expense of flow pressure is obtained as observed by the initial trend of increase in velocity at the orifice. However, decreasing the orifice diameter further resulted in a greater number of cavitation bubbles which led to bubble coalescence and hence the subsequent increase of Ca. Therefore, an optimized value of $L/d = 1.25$ is deemed ideal for our experimentation. Figure 4(a) and 4(b) denotes the contour plots from the simulation.

Furthermore, the L in the L/d ratio was varied to determine the ideal length of the orifice. A similar methodology was obtained and the velocity and pressure profiles are plotted in Supplementary Figure S2. There is a clear trend of velocity at the orifice increasing which is corroborated by the L/d vs. Ca plot (as L is varied) plotted in Figure 3(b). It is observed the Ca decreases as L is increased which leads to the increased extent of cavitation. However, the increasing L/d ratio has the effect of delaying the pressure recovery, and the low-pressure region is maintained through the length of the orifice. Subsequently, the predicted extent of the vapour cavity is shown to increase with the increasing L/d ratio under the same operating pressure conditions.

3.1.2. Effect of the pressure ratio

Another important parameter that determines the potency of a cavitating device is the inlet-to-outlet pressure ratio. The variation of Ca with the D/d ratio was also further investigated. This was done by keeping the orifice diameter constant and

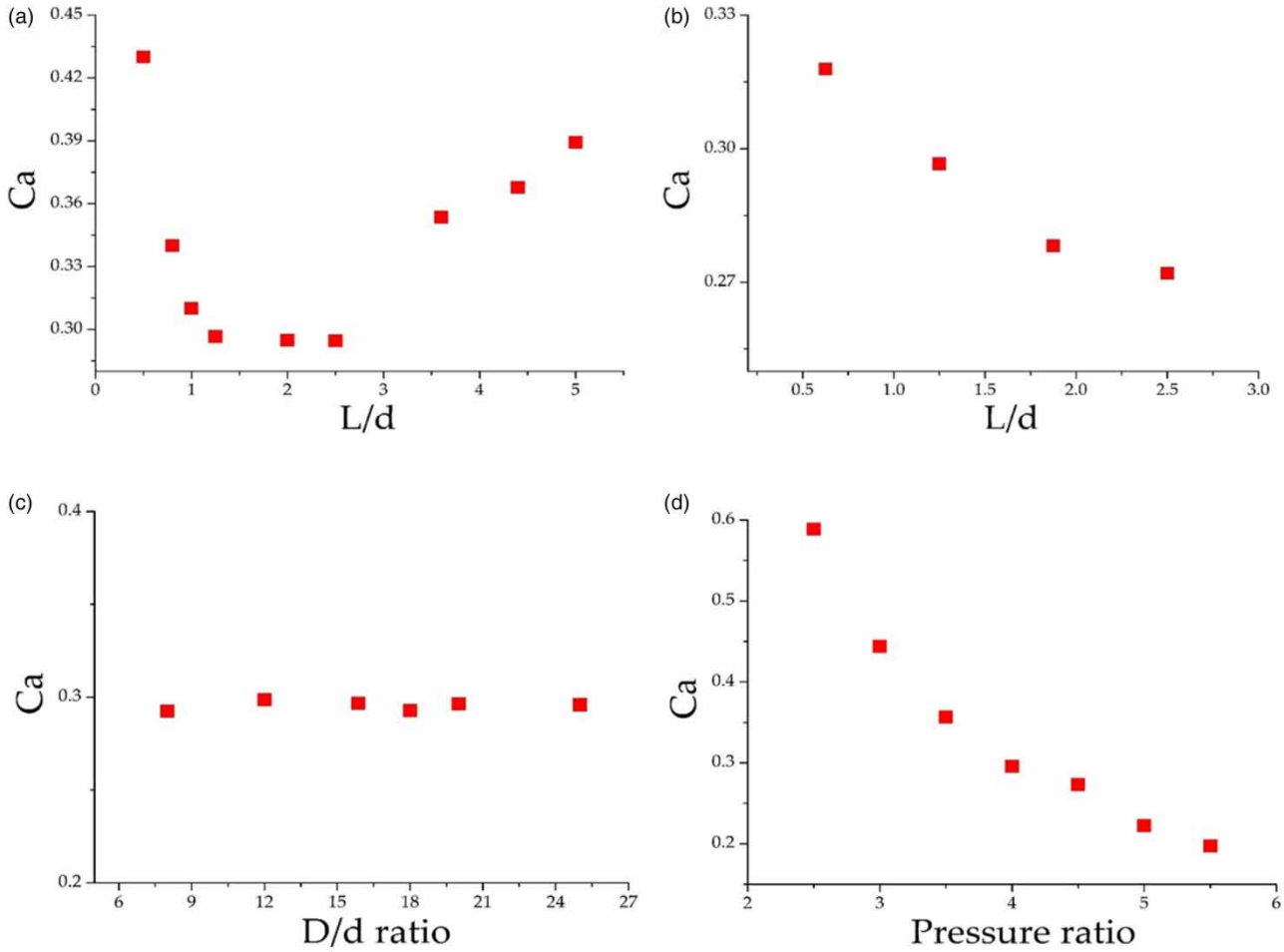

Figure 3 | Variation of cavitation number with (a) *L*/*d* (*d* varying), (b) *L*/*d* (*L* varying), (c) *D*/*d* and (d) pressure ratio.

varying the inlet pipe diameter from 12.8 to 40 mm. There were no significant variations observed in Ca with respect to the changes in inlet pipe diameter. This shows that there is no role of pipe diameter on the cavitation effect which is corroborated by Figure 3(c). Supplementary Figure S3 shows the variation of velocity profile while Supplementary Figure S4 denotes the pressure profiles with pressure ratios and Figure 3(d) shows the variation of cavitation numbers with the pressure ratio. It can be inferred from these plots is that for pressure ratios below 4, the pressure drop at the orifice constriction is not significant enough. Velocity profiles for varying pressure ratios have been denoted in Supplementary Figure S5 keeping *d* constant. At pressure ratio 4 and above, the pressure drop and therefore cavitation is significant. It is to be noted that pressure recovery is also significant at a pressure ratio 4 and above. Therefore, for our experimentation, as both pressure recovery and cavitation are shown to be significant at pressure ratio 4 such is adopted and experiments are performed keeping inlet pressure at 400,000 Pa.

3.2. Effect of process parameters

3.2.1. Effect of pH

pH of a solution is an essential factor in determining the performance efficiency of the cavitation process. In the present study, solution pH was varied from 2 to 10 and the results for the extent of NRF degradation are illustrated in Figure 5. It can be seen that the maximum degradation of around 22.26% was observed in pH 2 with a corresponding rate constant of $3.4 \times 10^{-3}\text{min}^{-1}$. The reason can be attributed to the fact that at acidic pH generation of hydroxyl radicals is more with less recombination reaction (Mukherjee *et al.* 2020a). As the pH changes from acidic to alkaline, it was found that the degradation efficiency decreases from 22.26 to 4% with a decrease in corresponding rate constants of 3.5×10^{-3} to

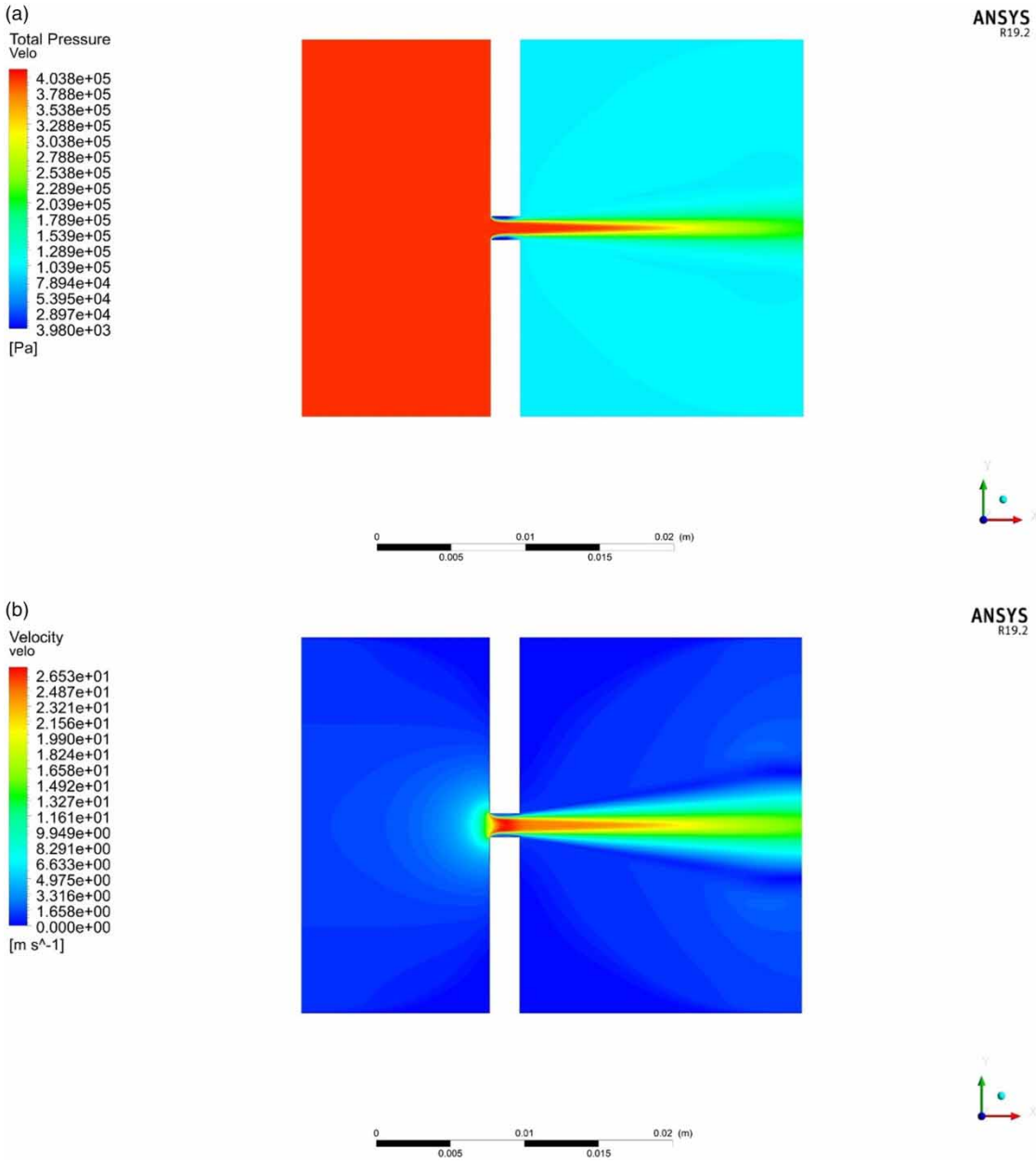

Figure 4 | Contour plots of (a) pressure and (b) velocity.

0.76×10^{-3}min^{-1}. It is because, under alkaline conditions, there is a higher number of •OH radical present in the solution, which under extreme conditions of cavitation bubble implosion undergo self-recombination and form H_2O_2 (Mukherjee *et al.* 2020b). Therefore, it can be concluded that at alkaline pH available hydroxyl radicals (main driving force for the cavitation-based approach) are limited. Hence, acidic pH is favourable for cavitation phenomena and pH 2 was considered to be optimum.

3.2.2. Effect of inlet pressure

Inlet pressure is another important process parameter for determining the efficiency of cavitation. Here, in this study, the pressure was varied between 4 and 7 bar and degradation is illustrated in Figure 6. At 4 bar pressure, a degradation of 13.76% was observed with a degradation rate constant of 2.2×10^{-3} min^{-1}. On further increasing the pressure to 5 and 6 bar, increased degradation of 17.98–22.26% and rate constant from 3.1×10^{-3} to 3.5×10^{-3} min^{-1} was recorded. An

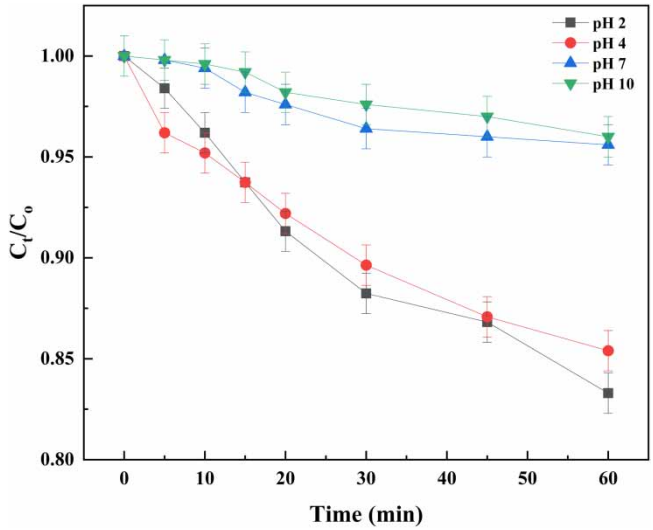

Figure 5 | Effect of solution pH on degradation of NRF.

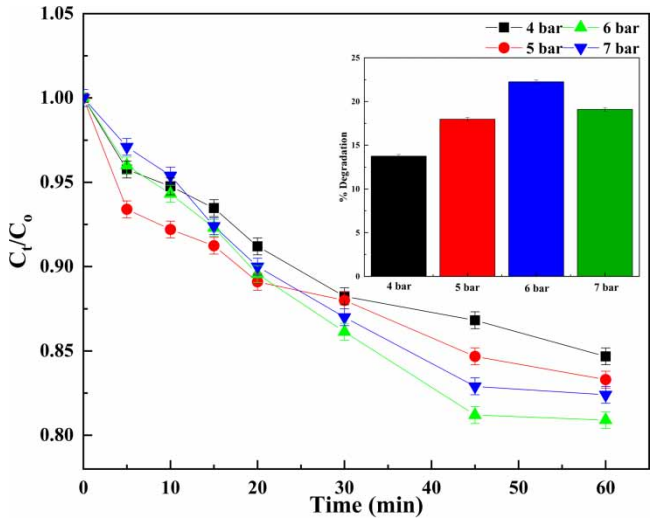

Figure 6 | Effect of pressure on degradation of NRF.

additional increase to 7 bar pressure the degradation extent reduces to 19.1% with a rate constant of 3.2×10^{-3}min^{-1}. The increase in the degradation is because of the increased cavitation intensity leading to higher hydroxyl radical formation and in turn higher degradation (Mukherjee *et al.* 2022b). Increasing the pressure beyond optimum leads to the generation of a higher number of cavity bubbles leading to a cavity cloud formation which further leads to decreased degradation (Patil & Baral 2021). Hence, 6 bar pressure was considered to be optimum.

3.2.3. Effect of initial concentration

Initial concentration is another important process parameter that determines the degradation performance in a cavitation process. In the present study, the initial concentration was varied from 200 to 300 μg/L keeping process parameters constant (such as pH – 2; orifice diameter – 1.6 mm; pressure – 6 bar). It can be observed that with an increase in initial concentration, degradation efficiency decreases (200 μg/L: 22.26%; 250 μg/L: 17.72%; 300 μg/L: 16.7%). The reason for a lower rate of degradation with increasing initial concentration can be attributed to the fact that while the concentration of NRF in the solution increases, the total contribution of hydroxyl radicals (•OH) remains constant (Joshi & Gogate 2012). Furthermore, the

obtained data were co-related assuming first-order kinetics based on the previous study conducted by Mukherjee *et al.* (2021b) and Saharan *et al.* (2012) for degradation of ciprofloxacin and dye pollutant, respectively. The degradation kinetics were calculated using Equations (10)–(13):

$$-\frac{d[\mathrm{NRF}]}{dt} = k[\mathrm{NRF}] \tag{10}$$

$$[\mathrm{NRF}] = [\mathrm{NRF}]_0 \exp[-kt] \tag{11}$$

$$\ln[\mathrm{NRF}] = -kt + \ln[\mathrm{NRF}]_0 \tag{12}$$

$$\ln\frac{[\mathrm{NRF}]}{[\mathrm{NRF}]_0} = -kt \tag{13}$$

where $[\mathrm{NRF}]_0$ is the initial concentration of MP and [NRF] is the concentration of MP at time t (mg/L), k is the degradation rate constant (min^{-1}) and t is the time (min). A linear fit of the experimental data from the logarithmic plot gives from the slope the k values. It was found that the data were well fitted by Equation (13) with a regression coefficient ~0.99 and the slope of the line, hence the degradation rate. The same trend was obtained for varying concentrations as well. Lastly, the plot of $\ln(C_t/C_0)$ vs. time shown in Figure 7 reveals the nature of the graph to be a straight line passing through the origin which confirms that NRF degradation follows first-order kinetics.

3.2.4. Performance of individual technologies

Degradation efficiency was calculated with other oxidizing agents' to evaluate the performance efficiency of each of the standalone technologies. For evaluation, the time and volume of studies were kept constant at 30 min and 50 L, respectively. It was observed that a degradation of 22.46% was obtained by using standalone HC, while using standalone ozonation, a maximum of 30.41% degradation was observed. On the other hand, degradation using standalone H_2O_2 and Fenton's reagent was found to be only 1.2 and 2.24%, respectively. The reason for the better performance of ozone can be attributed to the fact that ozone is an unstable compound with a relatively short half-life (Mukherjee *et al.* 2022c). However, certain limitations were observed in using the ozonation process which include its (i) high production cost, (ii) resistance to the local interfacial mass transfer during the injection of ozone from a stream of the gas mixture consisting of oxygen and ozone to the aqueous phase of the contaminated water, (iii) preferential reaction of O_3 with the sites with high electron density such as double bonds like C = C, C = N and N = N. Additionally, storage of ozone cannot be a viable method citing its low half-time of about 39 min; if used it needs to be produced at the location for higher effectiveness (Schaar *et al.* 2010). In view of this, it can be well

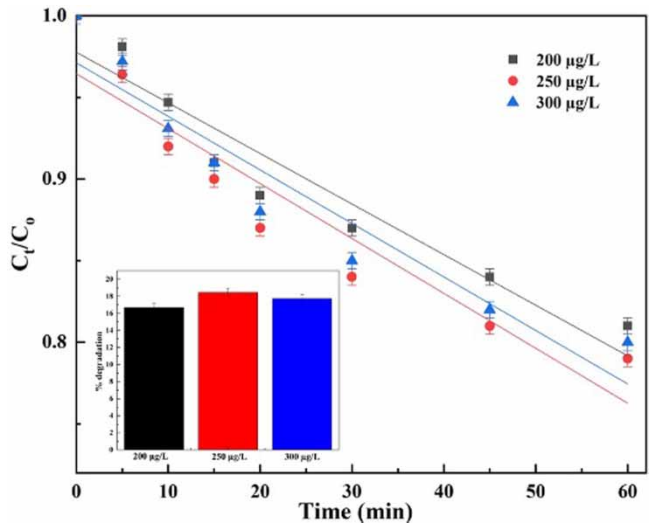

Figure 7 | C_t/C_0 values of degradation various initial concentration on the degradation of NRF (inset represents the variation in extent of degradation with initial concentration).

understood that cavitation-based treatment is a more sustainable, environmentally friendly, lower chance of harmful by-product formation and has easy implementation for scalability as compared to other AOP-based treatment processes.

3.3. Synergism effects of integrating oxidizing agents to HC process

3.3.1. Degradation efficiency of HC coupled with ozone

In the current study, synergism effects of integrating ozone to the cavitation system were also carried out to understand the process intensification. Ozone was injected into the system using a diffuser with varying ozone flow rates between 0.25 and 0.75 g/h for a time period of 30 min. At lower ozone dosage (0.25 g/h), a degradation of 62.06% with a degradation rate constant of 30.8×10^{-3} min^{-1} was observed. Subsequently, upon increasing the ozone dosage from 0.5 to 0.75 g/h, the maximum degradation increases from 66.6 to 70.48% with a rate constant from 35.8×10^{-3} to $39.8 \times 10^{-3} min^{-1}$ as illustrated in Figure 8. The reason can be attributed to the fact that under HC conditions, the ozone molecules overcome the mass transfer resistance in a gas-liquid system and are readily transformed into nascent oxygen and highly reactive hydroxide radicals (•OH) which further undergoes reaction in the aqueous media producing superoxide radicals ($\bullet O_2^-$) and hydroxide radicals (•OH) radicals (Cako *et al.* 2020) according to Equations (14)–(20)

$$H_2O \xrightarrow{HC} OH^{\cdot} + H^+ + e^- \quad (E^0 = 2.8V) \tag{14}$$

$$O_3 \xrightarrow{HC(2H^+ + 2e^-)} O_2^{\cdot} + H_2O \quad (E^0 = 2.08V) \tag{15}$$

$$O_3 \xrightarrow{HC} O_2 + O(^3P) \tag{16}$$

$$H_2O \xrightarrow{HC} OH^{\cdot} + {}^{\cdot}H \tag{17}$$

$$O(^3P) + H_2O \rightarrow 2HO^{\cdot} \tag{18}$$

$$HO^{\cdot} + O_2^- \rightarrow OH^- + {}^1O_2 \tag{19}$$

$$O_3 + OH^- \rightarrow HO_2^{\cdot} + O_2^{\cdot -} \tag{20}$$

$$O_2^{\cdot -} + NRF \rightarrow \text{degradation byproducts} \rightarrow CO_2 + H_2O$$

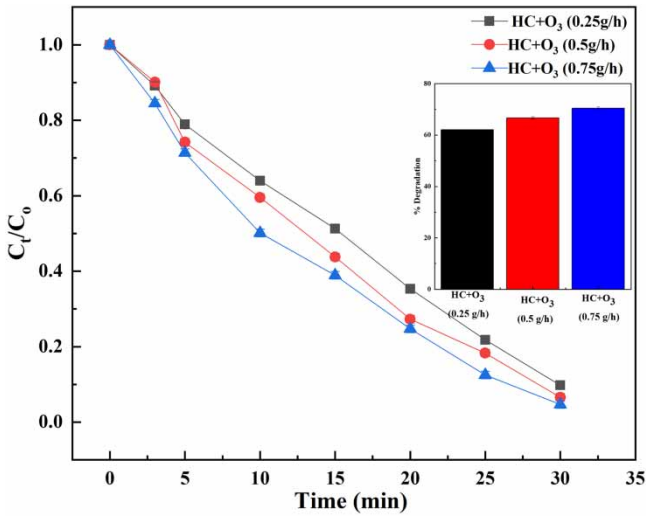

Figure 8 | Effect of O_3 on the degradation of NRF in conjugation with HC.

The synergistic coefficient for the ozone and HC coupled system is calculated in Equation (21). It can be observed that the overall efficiency of the combined system is higher than individual systems.

$$f = \frac{k_{HC+O_3}}{k_{HC} + k_{O_3}} = \frac{39.8 \times 10^{-3}}{3.4 \times 10^{-3} + 3.9 \times 10^{-3}} = 5.45 \quad (21)$$

3.3.2. Degradation efficiency of HC coupled with hydrogen peroxide

Hydrogen peroxide is a potent oxidizing agent with a potential of 1.8 V (Abdollahi & Hosseini 2014). The effect of the addition of H_2O_2 on the extent of degradation of NRF was studied by varying the concentration of hydrogen peroxide ranging from 0.1 to 0.5 g/L. The obtained results are depicted in Figure 9. It can be seen from the figure that upon increasing the dosage of H_2O_2 from 0.1 to 0.3 g/L, the extent of degradation of NRF increased from 45.7 to 58.48% with corresponding rate constant increases from 21.5×10^{-3} to $29.9 \times 10^{-3} min^{-1}$. This increase is because H_2O_2 dissociates into hydroxyl radicals which provide additional ·OH radicals leading to higher degradation (Sun *et al.* 2021). Furthermore, the cavitation phenomenon eliminates the mass transfer resistance due to generated local turbulence leading to effective utilization of H_2O_2 (Jain *et al.* 2019). Upon increasing H_2O_2 concentration to 0.5 g/L, a degradation of 55.76% with a rate constant of 24.9×10^{-3} min^{-1} was observed. This decrease in degradation may be attributed to (i) scavenging actions of residual H_2O_2 and (ii) recombination of excessive ·OH radicals leading to decreased cavitation performance (Mukherjee *et al.* 2020b). The synergistic coefficient for the H_2O_2 and HC coupled system is as calculated in Equation (22). It can be observed that the overall efficiency of the combined system is higher than individual systems.

$$f = \frac{k_{HC+H_2O_2}}{k_{HC} + k_{H_2O_2}} = \frac{57.8 \times 10^{-3}}{3.5 \times 10^{-3} + 2.2 \times 10^{-3}} = 10.14 \quad (22)$$

3.3.3. Degradation efficiency of HC coupled with Fenton's reagent

For understanding the degradation process by Fenton's reagent, experiments were conducted at different loadings of ferrous sulphate (1:1, 1:3 and 1:5) by keeping the dosage of H_2O_2 fixed at 0.3 g/L. As depicted in Figure 10 at H_2O_2:$FeSO_4$ 1:1, a degradation of 56.26% was obtained. Further increase in concentration of Fe to the ratio of 1:3 leads to increase in degradation to 64.48% and the rate of reaction from 29.9×10^{-3} to 37.1×10^{-3} min^{-1}. The increase in extent of degradation of NRF can be attributed to the generation of an enhanced quantum of hydroxyl radicals along with the cavitation effects (Mukherjee *et al.* 2020a). Further increase in Fe concentration to 1:5 leads to decrease in extent of degradation to 60.7%

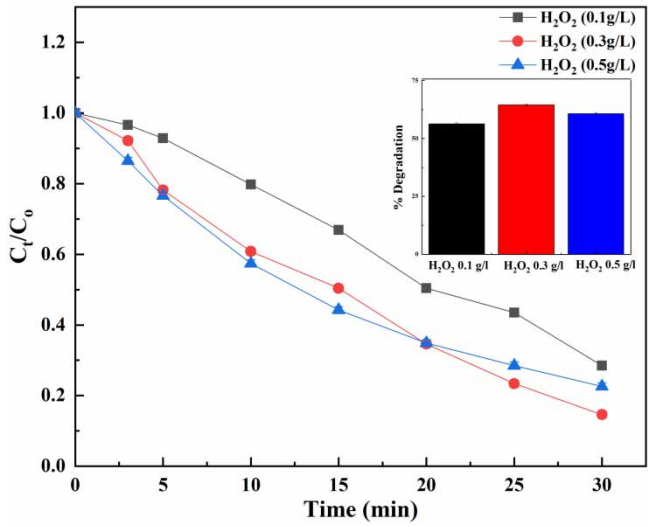

Figure 9 | Effect of H_2O_2 on the degradation of NRF in conjugation with HC.

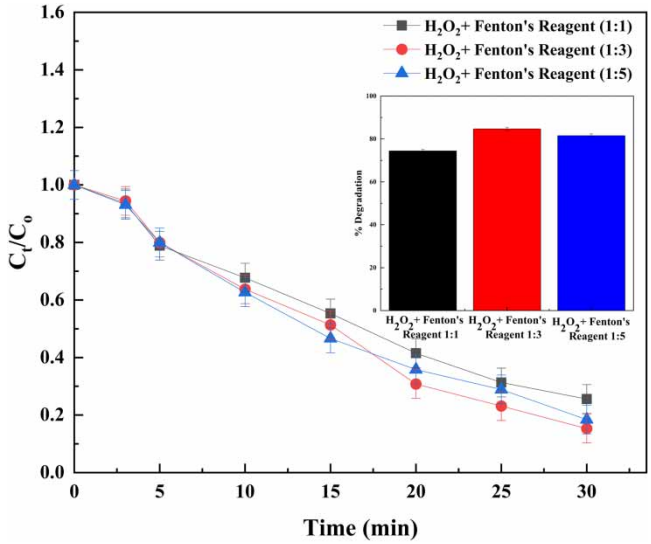

Figure 10 | Effect of Fenton's reagent on degradation of norfloxacin.

with corresponding rate constant to be 34.6×10^{-3} min^{-1}. This decrease is due to the scavenging phenomenon of H_2O_2 due to the recombination reaction (Patil *et al.* 2021). The synergistic coefficient for Fenton's reagent and HC coupled system is calculated in Equation (23). It can be observed that the overall efficiency of the combined system is higher than individual systems.

$$f = \frac{k_{HC+FR}}{k_{HC} + k_{FR}} = \frac{55.9 \times 10^{-3}}{3.5 \times 10^{-3} + 3.4 \times 10^{-3}} = 8.1 \quad (23)$$

4. ENERGY AND ECONOMICS

Developing sustainable and energy-efficient technology for the degradation of MP is a challenging task. Henceforth, energetic feasibility was carried out for the HC process to understand the techno-economic viability. For an HC process, cavitation yield (CY) is the most crucial parameter defined as the ratio of quantifiable effects of cavitation per unit energy supplied to the system (Mishra *et al.* 2022b). In addition, CY is interesting interplayed with energy consumption and economics. For an HC process, the major energy-consuming device is the pump. Table 1 represents the comparison of CY and economics of various processes involved. Additional cost of consumables (H_2O_2 and Fenton's reagent) and energy cost at Rs. 5.06/kWh (as per August 2021 data Telangana) has been considered while doing the calculations.

It can be observed from the table that standalone HC has the lowest CY of 0.0039 μg/J. Upon integration of HC with H_2O_2, O_3 and Fenton's reagent, CY has increased to 0.016, 0.007 and 0.017 μg/J. This is due to the synergistic effect as discussed in the previous section. The total energy consumption and time of operation have an inherent relation embedded and hence the discussion of both at the same time is crucially important. Standalone HC consumes the highest time of operation (180 min), hence consumes the highest energy (32.05 kWh). Integration of oxidizing agents results in reduction in time, hence a decrease in energy. Under the optimized conditions (discussed in the previous section), using H_2O_2 (dosage 0.3 g/L) consumes 8.01 kWh, while O_3 (dosage 0.75 g/h) consumes 26.13 kWh and Fenton's reagent (dosage 1:3 ratio) consumes 6.41 kWh. Finally, looking into the cost economics, it can be seen that HC consumes Rs. 160.57/m^3 which is the highest due to longer operational time. Using H_2O_2 (dosage 0.3 g/L) has an economics of Rs. 82.53/m^3, while Fenton's reagent (dosage 1:3 ratio) has an economics of Rs. 95.43/m^3. It was also observed that though ozone process enhances performance efficiency in a reduced time but shoots up the cost. Moreover, the addition of oxidizing agent results in a decrease in the cost but anything beyond a certain dosage is not a productive effort.

Table 1 | Comparison of cavitational yield and cost-effectiveness of various processes

Process	Time required for 95% degradation of NRF (in min)	Cavitational yield (μg/J)	Energy consumption for 95% degradation of NRF (kWh)	Total cost (including additives) (in Rs.)
HC	180	0.0039	32.05	160.57
HC + H_2O_2 (0.1 g/L)	45	0.012	8.01	75.53
HC + H_2O_2 (0.3 g/L)	45	0.016	8.01	82.53
HC + H_2O_2 (0.5 g/L)	45	0.015	8.01	87.53
HC + O_3(0.25 g/h)	35	0.006	26.13	120.78
HC + O_3(0.5 g/h)	35	0.006	26.13	125.29
HC + O_3(0.75 g/h)	35	0.007	26.13	130.95
HC + Fenton's (1:1)	45	0.015	6.41	87.73
HC + Fenton's (1:3)	45	0.017	6.41	95.43
HC + Fenton's (1:5)	45	0.016	6.41	103.43

5. CONCLUSION

The present study investigated the feasibility of HC as well as its integration with other AOPs for degradation of NRF, a recalcitrant MP discharged from the tertiary treatment point. Results from CFD studies were used to optimize the geometry of the orifice-based cavitating device. Primarily the objective of such optimization study is to keep conditions as favorable as possible for cavitation which is determined by Ca. However, CFD cannot accurately take into account choked cavitation or bubble coalescence which is an issue generally observed in laboratory scale and pilot plant studies. Further experimental studies showed that the operational parameters such as pH – 2, inlet pressure – 6 bar and initial concentration of 200 μg/L are favorable for the degradation of NRF. Furthermore, upon integration with oxidizing agents, it was found that the highest degradation efficiency was found in the following cases (a) HC + H_2O_2 (0.3 g/L): 58.48%, (b) HC + O_3 (0.75 g/h): 66.6%, (c) HC + Fenton's reagent (1:3 ratio): 60.48%. Interestingly, it was found that the addition of oxidizing agents resulted in a reduction in operation time. In this regard, it was also concluded that operational time plays a vital role in the energetics and economics of the process. The techno-economic study further revealed that HC + H_2O_2 consumed relatively less energy of 8.01 kWh/m^3 at the economics of Rs. 82.53/m^3. In a nutshell, it can be concluded that the designed cavitation process is a promising solution to the treatment of recalcitrant MP discharged from the tertiary effluent streams.

FUNDING

S.M. would like to thank DST-WTI Grant [Ref. DST/TMD/EWO/WTI/2K19/EWFH/2019/143] for carrying out the work (IICT/Pubs./2022/373).

DATA AVAILABILITY STATEMENT

All relevant data are included in the paper or its Supplementary Information.

CONFLICT OF INTEREST

The authors declare there is no conflict.

REFERENCES

Abdollahi, M. & Hosseini, A. 2014 Hydrogen peroxide. In: *Encycl. Toxicol*, 3rd edn, pp. 967–970. https://doi.org/10.1016/B978-0-12-386454-3.00736-3.

Cako, E., Gunasekaran, K. D., Cheshmeh Soltani, R. D. & Boczkaj, G. 2020 Ultrafast degradation of brilliant cresyl blue under hydrodynamic cavitation based advanced oxidation processes (AOPs). *Water Resour. Ind.* **24**. https://doi.org/10.1016/j.wri.2020.100134.

Chen, S., Li, Y., Lü, R. & Wang, P. 2013 Preparation, characterization of C/Fe-Bi_2WO_6 nanosheet composite and degradation application of norfloxacin in water. *J. Nanosci. Nanotechnol.* **13**, 5624–5630. https://doi.org/10.1166/JNN.2013.7486.

Das, R., Mukherjee, A., Sinha, I., Roy, K. & Dutta, B. K. 2020 Synthesis of potential bio-adsorbent from Indian Neem leaves (*Azadirachta indica*) and its optimization for malachite green dye removal from industrial wastes using response surface methodology: kinetics, isotherms and thermodynamic studies. *Appl. Water Sci.* **10**, 1–18. https://doi.org/10.1007/s13201-020-01184-5.

Department of Economic and Social Affairs n.d. Transforming our world: the 2030 Agenda for Sustainable Development. https://sdgs.un.org/2030agenda (accessed 19 July 2022).

Gogate, P. R. 2002 Cavitation: an auxiliary technique in wastewater treatment schemes. *Adv. Environ. Res.* **6**, 335–358. https://doi.org/10.1016/S1093-0191(01)00067-3.

Jain, P., Bhandari, V. M., Balapure, K., Jena, J., Ranade, V. V. & Killedar, D. J. 2019 Hydrodynamic cavitation using vortex diode: an efficient approach for elimination of pathogenic bacteria from water. *J. Environ. Manage.* **242**, 210–219. https://doi.org/10.1016/j.jenvman.2019.04.057.

Joshi, R. K. & Gogate, P. R. 2012 Degradation of dichlorvos using hydrodynamic cavitation based treatment strategies. *Ultrason. Sonochem.* **19**, 532–539. https://doi.org/10.1016/j.ultsonch.2011.11.005.

Kim, B. C., Pak, B. C., Cho, N. H., Chi, D. S., Choi, H. M., Choi, Y. M. & Park, K. A. 1997 Effects of cavitation and plate thickness on small diameter ratio orifice meters. *Flow Meas. Instrum.* **8**, 85–92. https://doi.org/10.1016/S0955-5986(97)00034-4.

Lanjewar, S., Mukherjee, A., Khandewal, P., Ghosh, A. K., Mullick, A., Moulik, S. & Roy, A. 2021 Thermodynamics of synthesis and separation performance of interfacially polymerized 'loose' reverse osmosis membrane: benchmarking for greywater treatment. *Chem. Eng. J.* **417**, 127929.

Lanjewar, S., Mishra, B., Mukherjee, A., Mullick, A., Moulik, S. & Roy, A. 2022 A critical review on prospects and challenges in 'conceptualization to technology transfer' for nutrient recovery from municipal wastewater. *Sustain. Water Treat.* 517–565. https://doi.org/10.1002/9781119480075.CH14.

Maddela, N. R., García Cruzatty, L. C., Leal-Alvarado, D. A., Olaya, J. C., Chakraborty, S. & Mukherjee, A. 2020 Quorum quenching for sustainable environment: biology, mechanisms, and applications. 73–112. https://doi.org/10.1007/978-981-15-2679-4_4.

Mishra, B., Mukherjee, A., Mullick, A., Bhandari, V. M. & Moulik, S. 2022a Design of hydrodynamic cavitation assisted intensified tertiary treatment unit for effective degradation of organic micropollutants in pharmaceutical industrial effluent: a case study with triclosan. *J. Water Process Eng.* **49**, 103132. https://doi.org/10.1016/j.jwpe.2022.103132.

Mishra, B., Thakare, A., Mukherjee, A., Mullick, A., Moulik, S. & Roy, A. 2022b Sustainable approach to biodiesel production using hydrodynamic cavitation route. *Environ. Sci. Eng.* 1093–1119. https://doi.org/10.1007/978-3-030-96554-9_73/COVER.

Mukherjee, A., Mullick, A., Teja, R., Vadthya, P., Roy, A. & Moulik, S. 2020a Performance and energetic analysis of hydrodynamic cavitation and potential integration with existing advanced oxidation processes: a case study for real life greywater treatment. *Ultrason. Sonochem.* **66**, 105116. https://doi.org/10.1016/j.ultsonch.2020.105116.

Mukherjee, A., Mullick, A., Vadthya, P., Moulik, S. & Roy, A. 2020b Surfactant degradation using hydrodynamic cavitation based hybrid advanced oxidation technology: a techno economic feasibility study. *Chem. Eng. J.* **398**, 125599. https://doi.org/10.1016/j.cej.2020.125599.

Mukherjee, A., Roy, A., Mullick, A. & Moulik, S. 2021a *Sustainable Technologies for Recycling Greywater: A Shift Towards Decentralized Treatment*. CRC Press.https://doi.org/10.1201/9781003052234-21.

Mukherjee, A., Satish, A., Mullick, A., Rapolu, J., Moulik, S., Roy, A. & Ghosh, A. K. 2021b Paradigm shift toward developing a zero liquid discharge strategy for dye-contaminated water streams: a green and sustainable approach using hydrodynamic cavitation and vacuum membrane distillation, ACS sustain. *Chem. Eng.* **9**, 6707–6719. https://doi.org/10.1021/acssuschemeng.1c00619.

Mukherjee, A., Mullick, A., Moulik, S. & Roy, A. 2021c Oxidative degradation of emerging micropollutants induced by rotational hydrodynamic cavitating device: a case study with ciprofloxacin. *J. Environ. Chem. Eng.* **9**, 105652. https://doi.org/10.1016/j.jece.2021.105652.

Mukherjee, A., Chalicheemala, S., Roy, S., Mullick, A., De, S., Roy, A. & Moulik, S. 2022a Design, development and performance evaluation of skid-mounted pilot wastewater treatment and resource recovery unit for mechanical scavenging vehicle. *J. Clean. Prod.* **371**, 133564. https://doi.org/10.1016/J.JCLEPRO.2022.133564.

Mukherjee, A., Teja, R., Mullick, A., Roy, S., Moulik, S. & Roy, A. 2022b Hydrodynamic cavitation: route to greener technology for wastewater treatment. *Sustain. Water Treat.* 57–115. https://doi.org/10.1002/9781119480075.CH3.

Mukherjee, A., Avisar, D. & Roy, A. 2022c Recent trends in ozonation technology: theory and application. *Sustain. Water Treat.* 117–170. https://doi.org/10.1002/9781119480075.CH4.

Nasiruddin, S. & Singh, S. N. 2021 Performance evaluation of an innovative design modification of an orifice meter. *Flow Meas. Instrum.* **80**, 101944. https://doi.org/10.1016/J.FLOWMEASINST.2021.101944.

Patil, A. D. & Baral, S. S. 2021 Process intensification of thumba methyl ester (Biodiesel) production using hydrodynamic cavitation. *Chem. Eng. Res. Des.* **171**, 277–292. https://doi.org/10.1016/J.CHERD.2021.05.007.

Patil, P. B., Bhandari, V. M. & Ranade, V. V. 2021 Wastewater treatment and process intensification for degradation of solvents using hydrodynamic cavitation. *Chem. Eng. Process. - Process Intensif.* **166**, 108485. https://doi.org/10.1016/j.cep.2021.108485.

Petrie, B., Barden, R. & Kasprzyk-Hordern, B. 2015 A review on emerging contaminants in wastewaters and the environment: current knowledge, understudied areas and recommendations for future monitoring. *Water Res.* **72**, 3–27. https://doi.org/10.1016/j.watres.2014.08.053.

Ricky, R. & Shanthakumar, S. 2022 Phycoremediation integrated approach for the removal of pharmaceuticals and personal care products from wastewater – a review. *J. Environ. Manage.* **302**, 113998. https://doi.org/10.1016/J.JENVMAN.2021.113998.

Roy, K., Mukherjee, A., Maddela, N. R., Chakraborty, S., Shen, B., Li, M., Du, D., Peng, Y., Lu, F. & Garciá Cruzatty, L. C. 2020 Outlook on the bottleneck of carbon nanotube in desalination and membrane-based water treatment – a review. *J. Environ. Chem. Eng.* **8**, 103572. https://doi.org/10.1016/J.JECE.2019.103572.

Saharan, V. K., Pandit, A. B., Satish Kumar, P. S. & Anandan, S. 2012 Hydrodynamic cavitation as an advanced oxidation technique for the degradation of Acid Red 88 dye. *Ind. Eng. Chem. Res.* **51**, 1981–1989. https://doi.org/10.1021/ie200249k.

Schaar, H., Clara, M., Gans, O. & Kreuzinger, N. 2010 Micropollutant removal during biological wastewater treatment and a subsequent ozonation step. *Environ. Pollut.* **158**, 1399–1404. https://doi.org/10.1016/J.ENVPOL.2009.12.038.

Simha, P. & Ganesapillai, M. 2017 Ecological sanitation and nutrient recovery from human urine: how far have we come? A review, Sustain. *Environ. Res.* **27**, 107–116. https://doi.org/10.1016/j.serj.2016.12.001.

Singhal, A. K., Athavale, M. M., Li, H. & Jiang, Y. 2002 Mathematical basis and validation of the full cavitation model. *J. Fluids Eng. Trans. ASME* **124**, 617–624. https://doi.org/10.1115/1.1486223.

Sun, X., You, W., Xuan, X., Ji, L., Xu, X., Wang, G., Zhao, S., Boczkaj, G., Yoon, J. Y. & Chen, S. 2021 Effect of the cavitation generation unit structure on the performance of an advanced hydrodynamic cavitation reactor for process intensifications. *Chem. Eng. J.* **412**, 128600. https://doi.org/10.1016/J.CEJ.2021.128600.

Zhang, A. & Li, Y. 2014 Removal of phenolic endocrine disrupting compounds from waste activated sludge using UV, H2O2, and UV/H2O2 oxidation processes: Effects of reaction conditions and sludge matrix. *Science of The Total Environment* **493**, 307–323.

First received 4 July 2022; accepted in revised form 25 March 2023. Available online 8 April 2023